Nonlinear Dyn
DOI 10.1007/s11071-016-2916-9

ORIGINAL PAPER

On the control and stability of variable-order mechanical systems

J. Orosco · C. F. M. Coimbra

Received: 20 January 2016 / Accepted: 19 June 2016

Abstract This work investigates the control and stability of nonlinear mechanics described by a system of variable-order (VO) differential equations. The VO behavior results from damping with order varying continuously on the bounded domain. A model-predictive method is presented for the development of a time-varying nominal control signal generating a desirable nominal state trajectory in the finite temporal horizon. A complimentary method is also presented for development of the time-varying control of deviations from the nominal trajectory. The latter method is extended into the time-invariant infinite temporal horizon. Simulation error dynamics of a reference configuration are compared over a range of damping coefficient values. Using a normal mode analysis, a fractional-order eigenvalue relation—valid in the infinite horizon—is derived for the dependence of the system stability on the damping coefficient. Simulations confirm the resulting analytical expression for perturbations of order much less than unity. It is shown that when deviations are larger, the fundamental stability characteristics of the controlled VO system carry dependence on the initial perturbation and that this feature is absent from a corresponding constant (integer or fractional) order system. It is then empirically demonstrated that the analytically obtained critical damping value accurately defines—for simulations over the entire temporal horizon—a boundary between rapidly stabilizing solutions and those which persistently oscillate for longtimes.

J. Orosco · C. F. M. Coimbra (✉)
Department of Mechanical and Aerospace Engineering,
Jacobs School of Engineering, University of California,
San Diego, CA, USA
e-mail: ccoimbra@ucsd.edu

J. Orosco
e-mail: jrorosco@ucsd.edu

Keywords Fractional derivative · Variable-order derivative · Stability · Nonlinear systems · Pendulum dynamics · Eigenvalue relation

1 Introduction

Some of the earliest contributions to applied fractional calculus were made by Oliver Heaviside in the last part of the nineteenth century (for a more complete historical account of the early development of Fractional Calculus see [31,34,38]).Within the framework of his operational calculus, Heaviside successfully described the behavior of electric transmission lines using the equivalent of fractional derivatives [31]. Since then, the analysis of physical phenomena with more complex constitutive relations has successfully employed fractional-order (FO) descriptions in a number of areas such as electrochemistry, biology, fluid mechanics, electronic circuits, geophysics, and rheology, among many others [1,11,12,16,26,30,33,44,46]. Aided in part by the availability of increasingly accurate experimental data, evidence of this behavior has been demonstrated empirically by several authors. Anastasio [1] showed that fractional differentiation can describe the

Published online: 30 June 2016

phase shift across frequencies observed in the activity of premotor neurons (a feature of FO systems dynamics demonstrated as a byproduct of the present work) and that fractional integration of the signal is successful in recovering the time series of this activity. Coimbra et al. [16] and L'Espérance et al. [26] have shown conclusively the relevance of fractional history effects in determining the motion of a particle in high-frequency low-Reynolds-number oscillatory flows. FO dynamics have also been shown to arise inherently in unsteady diffusive problems as described in [34] and [44].

It is well understood by control theorists that the modeling and control of dynamic systems are not separate issues, but should be interpreted together to arrive efficiently at a control solution. Thus, it makes sense that systems characterized by FO behavior—often, those possessing a strong 'memory' or characterized by response delays—stand to benefit from some form of FO control. Indeed, much work has been done recently in the analysis and control of FO systems toward this end. In [28], Lorenzo and Hartley demonstrated the importance of proper initialization of FO systems and expanded the theory in terms of initialization functions, denoting the result 'Initialized Fractional Calculus'. Charef et al. [13] described a method of singularity structures—composed of the superposition of pole-zero pairs on the negative real axis—that approximate fractional slopes on a log-log Bode plot. In [23], Hwang et al. propose two numerical methods for the inversion of FO Laplace transforms that provide some improvement in accuracy and convergence over the previous standard analytical and approximating inversion methods used in the solution of FO differential equations. Podlubny [35,36] described the generalization of the well-known integer-order PID controller to the FO $PI^{\lambda}D^{\mu}$ controller and demonstrated its benefit over its predecessor in the control of FO systems. Bagley and Calico [3] described the construction of FO state-space realizations for initially quiescent systems and described their solution in terms of the matrix Mittag-Leffler function. Hartley and Lorenzo [22] extended this work—within the framework of their Initialized Fractional Calculus—to systems with a nonzero initialization term, providing analysis of their stability in the w-plane (a transformation of the s-plane), and describing the expansion of traditional methods of control design to such systems. In [27], Li and Chen derive a FO linear-quadratic regulator for the optimal control of FO linear time-invariant systems. A more comprehensive review of current methods in the analysis and control of FO systems—including applications and an overview of the implementation of these methods in modern computing environments – is provided in [32].

An extension of FO systems, variable-order (VO) systems are those described by systems of differential equations containing at least one differintegral term whose order of differentiation is functionally dependent on the independent variable, the dependent variable, or some combination thereof. We call such operators variable-order differential operators (VODOs) and the differential equations utilizing these operators variable-order differential equations (VODEs). In comparison with FO systems, relatively little work has been done in the area of VO systems and operators. Until recently, the majority of the work in this topic was restricted to the mathematical characterization of proposed operators, as in the work of Samko and Ross [39,40]. In [29], Lorenzo and Hartley extend their earlier work in constant FO operators to those of VO, considering several possible definitions and investigating the mathematical properties associated with each (e.g., time dependence, nature and strength of memory, linearity, and semigroup adherence). Ingman et al. [24] proposed a VO integral operator for the description of the dynamics of a material whose behavior under loading varies in some continuous manner from elastic (order 0) to viscous (order 1), with order dependent on material state (which is itself dependent on time). Coimbra [15] defined a physically consistent VO differential operator and demonstrated its efficacy in describing physical processes by modeling an oscillating-mass system with variable viscoelastic damping. The resulting system description provided the first intuitive example of mechanics involving VODOs as modeled by consistent VODEs. Soon et al. [42] extended this work, developing a second-order accurate numerical method for the evaluation of the operator and for the solution of a class of VODEs. As with FO operators, the existence of many differing definitions for VODOs implies the need for careful selection of a given definition in accordance with the intended application. In [37], Ramirez and Coimbra discuss and compare a number of these definitions, establish a criteria for selection of an operator apt for the modeling of physical processes, and demonstrate the physical meaning of the operator that best fulfills these criteria. The interested reader is referred to [37] for a more complete description of the various VODO definitions and the conditions informing operator selection. Finally, Diaz and Coimbra [17,18] described the dynamics of nonlinear VO oscillators and investigated traditional modern control methods as applied to these systems.

In the present paper, we extend the work done in [17] to the well-known pendulum swing-up and stabilization problem in order to demonstrate a method for model-predictive control (MPC) of the VO system and for the time-varying control of deviations from the nominal trajectory generated by the MPC method. Further, a method for analytical derivation of the system stability with respect to the VO damping is presented and compared to simulations in the time-invariant stabilization phase. The result is then compared to the stability behavior of the controlled system over the entire temporal horizon in order to assess its adequacy in predicting the stability of the *entire* control solution as applied to the VO system.

1.1 A note on the inverted pendulum problem

The pendulum is a classical example of a simple nonlinear system and is prevalent in the nonlinear systems theory literature [19,25]. A direct extension of the simple pendulum to the arena of control theory is the inverted pendulum problem: maintaining an initially inverted pendulum about its upright, unstable equilibrium. Over the last five decades, the inverted pendulum problem and its variants have frequently served as token archetypal systems for the development of new methods of modeling, control, and estimation, and as benchmarks for the efficacy of newly developed methods [6,7,10,21,47]. This is because control of the inverted pendulum is a well-understood problem that incorporates the most fundamental aspects of modern control theory (e.g., control of nonlinear systems, state-space models, stability of controlled systems, control of time-varying and time-invariant systems, and finite- and infinite-horizon control), and because most variants of this problem can be experimentally verified in a laboratory setting with ease. A brief-yet-extensive review of the benchmark use of the inverted pendulum problem over the last 50 years is given in [6].

2 Operator selection

In what follows, we use the notation $d^{(\cdot)} f/\mathrm{d}\tau^{(\cdot)}$ and $\mathcal{D}^{(\cdot)} f$ interchangeably to mean the $(\cdot)$th derivative with respect to τ of the function f, choosing to be more explicit where necessary for the sake of mathematical clarity.

2.1 Variable-order differential operator (VODO)

To model the VO frictional effects, the VODO must produce physically meaningful results where the modeling of dynamic systems is concerned. Conditions governing selection of an operator fulfilling this requirement are given in [37]. Specifically, we require that the VODO should return the pth FO derivative when $q(t) = p$ over the whole domain of derivatives, including the extreme values. We also require the VODO to satisfy causality for all times since mechanical equilibrium. Thus, we use the Coimbra operator of VO q, valid for $q < 1$ [15]:

$$
{}_a\mathcal{D}_t^{q(t)} f(t) \triangleq \frac{1}{\Gamma(1-q(t))} \int_{a^+}^{t} (t-\tau)^{-q(t)} \frac{\mathrm{d} f(\tau)}{\mathrm{d}\tau} \mathrm{d}\tau + \frac{(f(a^+) - f(a^-)) t^{-q(t)}}{\Gamma(1-q(t))}, \tag{1}
$$

where $\Gamma(\cdot)$ is the Gamma function (generalized factorial function) and the second term is the initialization function for dynamic consistency of initial conditions departing from mechanical equilibrium. The initialization function is equal to zero only if the system is in mechanical equilibrium for t ranging from $-\infty$ to a^+. For $a = 0$, the initialization term evaluates to zero under the assumption that the system is equilibrium for all times $t < 0^+$. Although this definition is readily extended to any range of q, the above expression is well-suited for appropriately posed problems. This is to say that proper scaling of the dynamic model under consideration ensures the validity of the above definition over the domain of interest. A more involved characterization of this operator, along with a comparison to its approximation by multiple FO interpolations, is given in [15] and [42]. Of particular note is the fact that—as demonstrated in [42]—a properly weighted set of FOs converges to the VODO definition as the number of interpolating terms is increased. Other applications of the Coimbra operator can be found in [14,41,45,48,49].

2.2 Fractional-order differential operator (FODO)

For evaluation of the fractional derivative that arises in the stability analysis, we choose a standard Caputo definition. This choice avoids an unnecessarily complicated treatment of the initial conditions that may arise from definitions such as the Riemann-Liouville or Grünwald-Letnikov fractional derivatives. The Caputo derivative of constant FO p reads [35]

$$ {}_a^C\mathcal{D}_t^p f(t) \triangleq \frac{1}{\Gamma(m-p)} \int_a^t (t-\tau)^{m-p-1} \frac{d^m f(\tau)}{\mathrm{d}\tau^m} \mathrm{d}\tau, \tag{2} $$

where $m-1 < p < m$ for $m \in \mathbb{Z}^+$, and with initial time a. As noted in [35], the Caputo fractional derivative and the more commonly encountered Riemann-Liouville fractional derivative are equivalent when the lower limit is taken as $a \to -\infty$, corresponding to each operator having equivalent steady-state behavior. A more intuitive explanation of this result is that the two definitions approach equivalence as memory of the initial condition approaches zero. It is therefore important when distinguishing between the two definitions to note the difference in how the initial conditions of each are expressed. The Laplace transform of each operator (see, e.g., [35]) reveals that the Riemann-Liouville definition has initial conditions of FO, whereas the initial conditions of the Caputo definition are of integer order. The physically meaningful interpretation of the initial conditions of the Caputo definition makes it the preferred operator when modeling physical processes. Additionally, use of the Caputo definition is consistent for this work, since the Caputo fractional operator is fully consistent with the Coimbra VO operator.

2.3 Numerical evaluation of VODO and FODO

Numerical differintegration of the VODO is achieved by the quadrature method applied within the framework of the generalized trapezoidal rule as described in [2], with the result given in [42] as

$$ \begin{aligned} \mathcal{D}^q f_n = & \frac{h^{1-q}}{\Gamma(3-q)} \sum_{i=0}^{n} \varphi_{i,n} \mathcal{D}^1 f_i \\ & + \frac{(f_{0^+} - f_{0^-})(t_n)^{-q}}{\Gamma(1-q)}, \end{aligned} \tag{3} $$

for a grid of uniform step size h and with the quadrature weighting

$$ \varphi_{i,n} = \begin{cases} (n-1)^{2-q} - n^{1-q}(n+q-2), & \text{if} \quad i=0, \\ (n-i-1)^{2-q} - 2(n-i)^{2-q} & \\ \quad +(n-i+1)^{2-q}, & \text{if} \quad 0 < i < n, \\ 1, & \text{if} \quad i=n, \end{cases} \tag{4} $$

where we have taken the lower terminal to be $\tau = a = 0$ for initialization of the operator. Though the numerical treatment of the operator is second order, we utilize a fourth-order Runge–Kutta (RK4) method for the simulations that follow. This includes the numerical solution to the differintegral state-space equations as well as the matrix differential Riccati equation. As an example, we consider the system

$$ E(\boldsymbol{x})\dot{\boldsymbol{x}} = N(\boldsymbol{x}, \boldsymbol{u}), \tag{5} $$

where $N(\cdot)$ is some nonlinear function of the states and control input, and $E(\cdot)$ allows for the flexible modeling of a broader class of problems (the latter can be set to the appropriately sized identity matrix as dictated by the system to be modeled). Defining

$$ \mathcal{R}(\boldsymbol{x}, \boldsymbol{u}) \triangleq E(\boldsymbol{x})^{-1} N(\boldsymbol{x}, \boldsymbol{u}), \tag{6} $$

the RK4 method at the k^{th} iteration is given by

$$ \begin{aligned} \boldsymbol{\delta_1} &= \mathcal{R}(\boldsymbol{x_k}, \boldsymbol{u_k}), \\ \boldsymbol{\delta_2} &= \mathcal{R}(\boldsymbol{x_k} + (h/2)\boldsymbol{\delta_1}, \boldsymbol{u_k}), \\ \boldsymbol{\delta_3} &= \mathcal{R}(\boldsymbol{x_k} + (h/2)\boldsymbol{\delta_2}, \boldsymbol{u_k}), \\ \boldsymbol{\delta_4} &= \mathcal{R}(\boldsymbol{x_k} + h\boldsymbol{\delta_3}, \boldsymbol{u_k}), \\ \boldsymbol{\Delta} &= (\boldsymbol{\delta_1} + \boldsymbol{\delta_4})/6 + (\boldsymbol{\delta_2} + \boldsymbol{\delta_3})/3, \\ \boldsymbol{x_{k+1}} &= \boldsymbol{x_k} + h\boldsymbol{\Delta}, \end{aligned} \tag{7} $$

where h is the step size of the temporal discretization and $\boldsymbol{\Delta}$ represents the RK4 step direction.

Further, noting that the Coimbra VODO yields the appropriate pth-order derivative when $q(t) = p$, and under the condition that the system is in equilibrium for $t < 0^+$ (i.e., that the initialization term evaluates to zero), we arrive at the numerical evaluation of the Caputo definition (that is, of the FODO) by setting $q(t) \equiv p$ in Eq. (3).

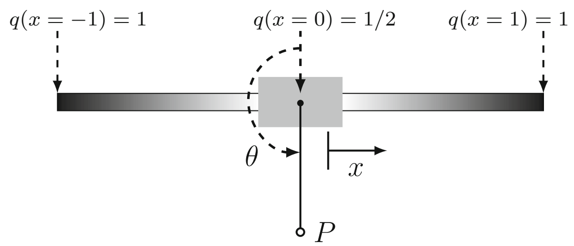

Fig. 1 The inverted pendulum problem at $t = 0$. The pendulum tip is denoted P, with $\theta = \pi$. The *gray rectangle* represents the cart, which moves linearly along the track in the direction x. The long thin *rectangle* represents the track, which is coated in a thin film of nonuniform material composition such that the damping order q is dependent on the position of the cart. The *shading* represents a continuum of damping order bounded by the values: $q(x) = 1$ (viscous) at the ends (*black*) and $q(x) = 1/2$ (viscoelastic) at the center (*white*)

3 Problem description

Consider a pendulum attached at one end to the center of a cart (Fig. 1). The cart moves linearly on a horizontal track, and the pendulum is free to rotate about its pivot. Only the linear motion of the cart is controlled.

The track is coated in a thin film of nonuniform material composition such that its damping behavior is represented in the model as varying continuously from viscoelastic (order 1/2) at the center to purely viscous (order 1) near the ends of the track.

The system is constrained by the dynamic model and by some combination of given parameters (e.g., track length and pendulum mass). We wish to determine a nominal control that will take the pendulum from a resting (downward hanging) position to an upright, stabilized position. We also seek a feedback law to correct for small deviations from the nominal trajectory during both the swing-up and stabilization phases.

In what follows, we designate the interval of time over which the swing-up portion of the problem occurs the 'finite horizon' and that over which the upright stabilization occurs the 'infinite horizon'.

3.1 Model

The equations of motion governing this classical problem are well-known and available in dynamics modeling and control texts such as [5], as well as in studies conducted for various control schema applied to this system such as, e.g., [7,47]. Adaptation of these equations to include the VO damping effects yields the system of nonlinear VODEs

$$
\begin{aligned}
&(m_c + m_p)\frac{d^2x}{dt^2} - m_p l_p \cos\theta \frac{d^2\theta}{dt^2} \\
&\quad + m_p l_p \sin\theta \left(\frac{d\theta}{dt}\right)^2 = v - c_0(x)\mathcal{D}^{q(x)}x, \\
&\quad - m_p l_p \cos\theta \frac{d^2x}{dt^2} + (\mathcal{I}_p + m_p l_p^2)\frac{d^2\theta}{dt^2} \\
&\quad - m_p g l_p \sin\theta = 0,
\end{aligned}
\tag{8}
$$

where $\mathcal{D}^{q(x)}$ is the Coimbra VODO and the parameters of the system are: $x(t)$, the cart position (relative to the track center); $\theta(t)$, the pendulum position (counterclockwise relative to upright); $v(t)$, the control signal; $c_0(x)$, the frictional coefficient; m_c, the cart mass; m_p, the pendulum mass; l_p, the pendulum half-length; l_t, the track length; $\mathcal{I}_p$, the pendulum mass moment about its center of mass; and g, gravity.

We take the characteristic scales $\mathcal{M}_c = m_c + m_p$, $\mathcal{L}_c = l_t/2$, and $\mathcal{T}_c = 2\pi\sqrt{(2l_p)/g}$, where $\mathcal{T}_c$ is equivalent to the natural period of the pendulum. Defining the dimensionless parameters

$$
\begin{aligned}
\xi &\triangleq x/\mathcal{L}_c, \\
\tau &\triangleq t/\mathcal{T}_c, \\
u &\triangleq v(\mathcal{T}_c^2/\mathcal{L}_c\mathcal{M}_c), \\
c &\triangleq c_0/(\mathcal{M}_c\mathcal{T}_c^{2-q}), \\
m &\triangleq m_p/\mathcal{M}_c, \\
l &\triangleq l_p/\mathcal{L}_c, \\
\gamma &\triangleq (ml)(g/(\mathcal{L}_c/\mathcal{T}_c^2)),
\end{aligned}
\tag{9}
$$

and the auxiliary dimensionless parameters

$$
\begin{aligned}
\mathcal{T} &\triangleq -ml, \\
\mathcal{I} &\triangleq (4/3)ml^2,
\end{aligned}
\tag{10}
$$

(corresponding to a dimensionless torque and dimensionless inertial moment, respectively), the system is cast in dimensionless form as

$$
\begin{aligned}
&\frac{d^2\xi}{d\tau^2} + \mathcal{T}\cos\theta\frac{d^2\theta}{d\tau^2} = \mathcal{T}\sin\theta\left(\frac{d\theta}{d\tau}\right)^2 \\
&\quad + u - c\mathcal{D}^{q(\xi)}\xi, \\
&\mathcal{T}\cos\theta\frac{d^2\xi}{d\tau^2} + \mathcal{I}\frac{d^2\theta}{d\tau^2} = \gamma\sin\theta.
\end{aligned}
\tag{11}
$$

We consider a quadratic distribution of the VO frictional effects given by $q(\xi(t)) = (1+\xi(t)^2)/2$, so that the variable derivative order is always less than unity on the bounded domain. We will also take c constant for the present analysis, noting that, in general, c may be a function of the cart position. Finally, the temporal boundary distinguishing the finite and infinite horizons is henceforth denoted $\tau = T$.

4 Methods

In order to develop control solutions, the model is quasilinearized, leaving the VO term in nonlinear form. The nominal control and nominal trajectory are developed using an adjoint-based minimization method with a combination of the linear and nonlinear model dynamics. Optimal control of deviations from the nominal trajectory is then formulated from the linearized portion of the quasilinearized system, regarding the VO damping term as a nonlinear state disturbance.

The two proposed methods (one for time-invariant systems and one for time-varying systems) are an extension of existing (well-established and fairly ubiquitous) methods for the control of constant integer-order differential equations. The general nonlinear form of the state-space equation given in the section to follow can be used to model a broad class of problems defined by smooth VODEs. This includes ordinary differential equation discretizations of partial differential systems [5]. This is to say that the methods are independent of the pendulum problem, which is used here only to demonstrate the utility of the proposed methods.

As the entirety of the underlying mathematics for such a method can be found in many graduate level controls texts, and the purpose of this work is to demonstrate the assimilation of VO dynamics and control into an existing (and well-documented) mathematical framework, we provide here a *concise* summary of these mathematics as applied to the system under investigation.

4.1 Quasilinearized state-space model

Defining the dimensionless state vector

$$\boldsymbol{\xi} \triangleq \left(\xi \;\; \theta \;\; \frac{d\xi}{\mathrm{d}\tau} \;\; \frac{\mathrm{d}\theta}{\mathrm{d}\tau} \right)^{\top}, \tag{12}$$

we can express Eq. (11) in the state-space form

$$E\mathcal{D}^1\boldsymbol{\xi} = N(\boldsymbol{\xi}, u) + F\mathcal{D}^q\xi, \tag{13}$$

which has the quasilinearization

$$\bar{E}\mathcal{D}^1\boldsymbol{\xi} = A\boldsymbol{\xi} + Bu + F\mathcal{D}^q\xi, \tag{14}$$

where the matrices E and N are easily obtained by inspection (see, e.g., [5]), the matrices A and B are obtained as a linearization of N about some nominal $\bar{\boldsymbol{\xi}}$ and $\bar{u}$, the matrix $\bar{E} = E(\bar{\boldsymbol{\xi}})$, and $F = [0 \;\; 0 \;\; -c \;\; 0]^{\top}$.

The state-space representation in Eq. (14) is a quasilinear VO differential (in fact, integrodifferential) equation. Sufficient conditions for local controllability of equations of this type in Banach spaces have been described in [4]. The term $F\mathcal{D}^q\xi$ is bounded, and the linear control of quasilinear systems subject to bounded nonlinear state-dependent perturbations has been recently studied [8,9,43]. We thus proceed with the development of a linear control schema, treating the frictional term as a bounded nonlinear state-dependent disturbance.

4.2 Model-predictive control

We define the quadratic cost function

$$J(\boldsymbol{u}) \triangleq \frac{1}{2}\int_0^T (\boldsymbol{\xi}^{\top} Q\boldsymbol{\xi} + \boldsymbol{u}^{\top} R\boldsymbol{u})\mathrm{d}\tau + \frac{1}{2}(E\boldsymbol{\xi})^{\top} Q_T E\boldsymbol{\xi}, \tag{15}$$

with $Q \geq 0$, $R > 0$, and $Q_T \geq 0$ being penalty (weighting) matrices used to tune the control response for the state trajectory, control effort, and terminal state, respectively. Since this method is an iterative descent method, the requirement for the R matrix is relaxed to $R \geq 0$. For the optimal control methods that follow (which require the invertibility of R) the strict condition holds. The terminal penalty matrix is, in particular, useful in the determination of an appropriate nominal control during the model-predictive process, since the finite-horizon control solution must 'hand over' a final state at $\tau = T$ that is tractable for the infinite-horizon control solution on the interval $\tau \geq T$. By considering small perturbations, $\boldsymbol{u}'$, to the control input that result in small perturbations, $\boldsymbol{\xi}'$, to the system trajectory, and developing the perturbation and adjoint equations, it is readily shown that (cf. [5]) the gradient, $\boldsymbol{g}$, of J with respect to $\boldsymbol{u}$—and constrained by the undisturbed system dynamics in Eq. (14)—is given by

$$\boldsymbol{g} = B^{\top}\boldsymbol{r} + R\boldsymbol{u}, \tag{16}$$

where $\boldsymbol{r}$ is the costate, and its terminal condition is given by $\boldsymbol{r}(T) = Q_T E\boldsymbol{\xi}(T)$. The costate adheres to the dynamics described by the adjoint equations, which are developed using the linearized portion of the system dynamics. The adjoint equations are dependent on $\boldsymbol{\xi}$, so that in order to determine the gradient, one must first obtain the state trajectory using the full nonlinear dynamics. Accordingly, generation and optimization of the nominal control and nominal state trajectory are achieved as follows:

1. guess an initial value for the control on $\tau \in [0, T]$ and step the state forward through the interval using the *full nonlinear dynamics* of Eq. (13);
2. using the terminal condition on $\boldsymbol{r}$, step the adjoint system backward from $\tau = T$ using the *linearized adjoint equations* developed from the linear portion of the quasilinearized dynamics described by Eq. (14);
3. compute the gradient and update the control using an appropriate conjugate gradient method;
4. iterate until some convergence criteria is met (or until a desirable nominal trajectory is obtained); and
5. store the resulting nominal control and state trajectory, denoted $\boldsymbol{u_n}$ and $\boldsymbol{\xi_n}$, respectively.

4.3 Optimal control

Subsequent to the development of the model-predictive control signal, it is necessary to derive a feedback law to be applied to errors between the nominal trajectory and the actual trajectory. Letting $\boldsymbol{\xi_p}(\tau) \triangleq \boldsymbol{\xi}(\tau) - \boldsymbol{\xi_n}(\tau)$ and $\boldsymbol{u_p}(\tau) \triangleq \boldsymbol{u}(\tau) - \boldsymbol{u_n}(\tau)$ be the state and control errors, respectively, we define the quadratic cost function

$$\begin{aligned} J(\boldsymbol{u_p}) \triangleq \frac{1}{2}\int_0^T (\boldsymbol{\xi_p}^{\top} Q \boldsymbol{\xi_p} + \quad & \boldsymbol{u_p}^{\top} R \boldsymbol{u_p})\mathrm{d}\tau \\ + \frac{1}{2}(E\boldsymbol{\xi_p})^{\top} Q_T E\boldsymbol{\xi_p}, \end{aligned} \tag{17}$$

which is a functional on the error energy of the controlled system that includes a penalty on the terminal state error. Following the same procedure outlined in Sect. 4.2 to develop the gradient, we now use a direct method. Setting the gradient equal to zero, we may write [5]

$$\boldsymbol{u_p} = K\boldsymbol{\xi_p}, \tag{18}$$

where

$$K = -R^{-1}B^{\top}XE \tag{19}$$

is the optimal feedback gain matrix and the determination of X is achieved by solving the appropriate matrix Riccati equation in the finite or infinite horizon as needed.

4.3.1 Finite horizon

In the finite horizon, $X = X(\tau)$ is the solution to the *differential* Riccati equation

$$\frac{\mathrm{d}X}{\mathrm{d}\tau} = -(\tilde{A}^{\top}X + X\tilde{A} - XBR^{-1}B^{\top}X + \tilde{Q}), \tag{20}$$

where $\tilde{A} \triangleq A\bar{E}^{-1}$, $\tilde{Q} \triangleq \bar{E}^{-\top}Q\bar{E}^{-1}$, and both A and $\bar{E}$ are time-varying. The total control solution for $\tau \in [0, T]$ is then given by

$$\begin{aligned} \boldsymbol{u}(\tau) &= \boldsymbol{u_n}(\tau) + \boldsymbol{u_p}(\tau), \\ &= \boldsymbol{u_n}(\tau) + K_f(\tau)\boldsymbol{\xi_p}(\tau), \end{aligned} \tag{21}$$

with K_f being the time-varying optimal feedback gain matrix on the finite horizon, determined as in Eq. (19).

4.3.2 Infinite horizon

In the infinite horizon, the solution, $X = X(\tau)$, can be obtained by solving the differential Riccati equation for $\tau \to \infty$. This is equivalently the constant solution, X, to the *algebraic* Riccati equation

$$0 = A^{\top}X\bar{E} + \bar{E}^{\top}XA - \bar{E}^{\top}XBR^{-1}B^{\top}, \tag{22}$$

where A and $\bar{E}$ are now time invariant. The nominal trajectory is identically null for $\tau \geq T$, so that $\boldsymbol{u_n} \equiv \boldsymbol{0} \ \forall \ \tau \in [T, \infty)$ and the resulting control solution is

$$\begin{aligned} \boldsymbol{u}(\tau) &= \boldsymbol{u}_{\boldsymbol{p}}(\tau), \\ &= K_i \boldsymbol{\xi}_{\boldsymbol{p}}(\tau), \end{aligned} \tag{23}$$

with K_i being the time-invariant optimal feedback gain matrix on the infinite horizon, determined as in Eq. (19).

5 Simulations

In light of the large number of parameters available for tuning the controller, it is desirable to define a basic configuration that is in some sense robust to the variation in the frictional coefficient. We choose the following for the physical parameters of the system: $g = 9.81$, $l_t = 2$, $m_c = 1$, $m_p = 0.05$, and $l_p = 0.15$. The units are SI. Parameters for the simulation were selected to reflect realistic conditions given the nature of the problem. For the temporal discretization, the numerical step size $h = 0.01$ was used. We let the boundary between the finite and infinite horizons be $\tau = T = 2$. When $\tau = T$, the nominal trajectory resulting from the pendulum swing-up is not the state-space origin, so that the upright stabilization phase is automatically subject to an initial perturbation requiring control corrections in the infinite horizon. Regardless, we introduce a perturbation to the initial state given by

$$\boldsymbol{\xi}(0) = \begin{pmatrix} -0.1 \\ \pi - 0.1 \\ 0 \\ 0 \end{pmatrix}, \tag{24}$$

so that the efficacy of the time-varying error correcting control signal over the finite horizon may also be observed. Finally, we take the basic tuning configuration $Q = diag(0, 0, 0, 0)$, $R = 0$, and $Q_T = diag(20, 12, 0.1, 20, 000)$ for generation of the nominal control using the model-predictive methods of Sect. 4.2. Doing so yields a state at $\tau = T$ which is stable to a range of frictional values when all subsequent tuning parameters set to unity or the appropriately sized identity matrix. That is, by a judicious choice of the parameters used to develop the nominal trajectory, the control solution for the error dynamics can then be developed as though there is *no weighting* applied to the states or to the control in the cost functional, so that the feedback law is everywhere a result of a direct measure of the systemic error energy. In the analysis to follow, no effort is made to tune the controller beyond the basic defined configuration. This provides a reference for comparison of the system dynamics over the investigated frictional values. With the system configured as described, the method produces a stabilizing solution on the bounded domain for $c \in [0, 1.89]$. Simulations were conducted on this interval with a frictional step size $\Delta c = 0.01$.

5.1 Controlled dynamics

The stable system dynamics for $c = 0$ are given in Fig. 2. This corresponds to the classical problem without the modeling of frictional effects. The pendulum swing-up phase is accomplished in $\tau = T = 2$ dimensionless time steps, moving through two periods of oscillation during that time. Since a single time step corresponds to the natural period of the pendulum, the nondimensionalized model is evidently self-consistent. Figure 3 gives the error dynamics of the system at the extreme values of the investigated frictional interval. When $c = 0$, we have the classical single pendulum swing-up solution: After swing-up, the system is quickly and smoothly brought to the origin of the state space. When $c = 1.89$, the system approaches a stability boundary: the dynamics oscillate in a persistent manner, decaying only after a very longtime ($\tau \gtrsim 300$). In fact, this tends to be so for all $c \gtrsim 1.73$, a result that is investigated further in the sections that follow.

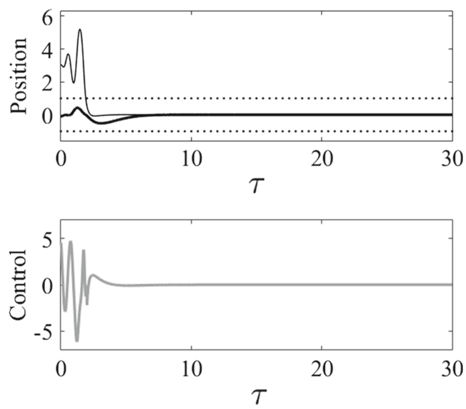

Fig. 2 *Top* dynamics of the controlled system with $c = 0$ and the initial perturbation given by Eq. (24): cart position (*thick solid*), pendulum position (*thin solid*), and domain boundaries (*dotted*). *Bottom* the control signal generating the desired state trajectory. Optimal control of deviations from the nominal trajectory is generated with weighting parameters set to unity or the appropriately sized identity matrix

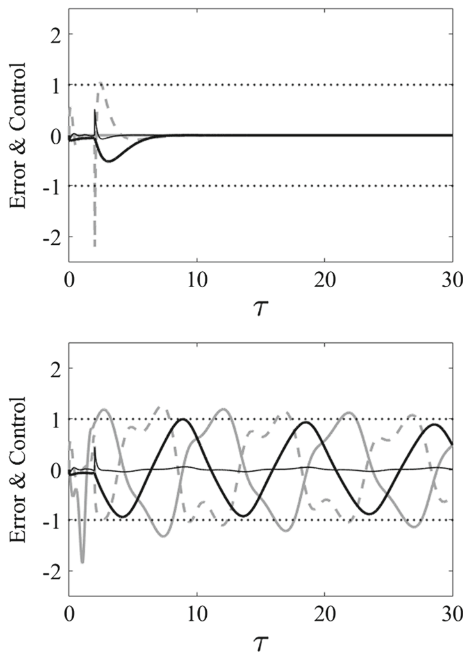

Fig. 3 Error dynamics and control. *Top* $c = 0$, corresponding to the classical problem without frictional forces. *Bottom* $c = 1.89$, corresponding to the largest frictional value valid on the domain. In each *plot* pendulum position error (*thin solid black*), cart position error (*thick solid black*), error control (*dashed gray*), frictional force (*solid gray*), and domain boundary (*dotted black*)

5.2 Phase plots

We choose $c = 0.01$ with $\tau \in [0, 10]$ and $c = 1.89$ with $\tau \in [0, 100]$ for generation of the cart position phase plots in Figs. 4 and 5. The value $c = 0.01$ is chosen to represent the lower extreme frictional value so that the VO phase space has meaning. From the phase diagrams, it appears that—over 'reasonable' time periods—the system will tend to stabilize to the state-space origin at lower frictional values and tend toward persistent oscillation for larger frictional values. By 'reasonable', we refer to time periods that make sense given the context of the problem. The apparent limit cycle in Fig. 5 is not a true limit cycle, since, as previously noted, the oscillations eventually decay after a very longtime. In the stability analysis to follow, it is shown that this is due to the nonlinear, memory-laden nature of the VO effects, which tend to stabilize the system dynamics.

The phase portrait depicting $D^{q(\xi)}\xi$ vs. ξ represents the variable phase space of the system. It is clear that the VO phase diagram is a nonlinear composition of the

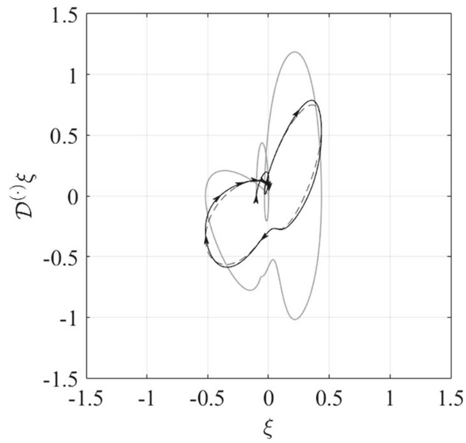

Fig. 4 Phase plot for $c = 0.01$ with $\tau \in [0, 10]$. *Arrows* plotted at intervals of $\Delta\tau = 1$ indicate direction of forward moving time. Shown: $\mathcal{D}^1\xi$ versus ξ (*solid gray*), $\mathcal{D}^{1/2}\xi$ vs. ξ (*dashed black*), and $\mathcal{D}^{q(\xi)}\xi$ vs. ξ (*solid black*). The VO phase diagram is a nonlinear composition of the order 1 and order 1/2 phase diagrams

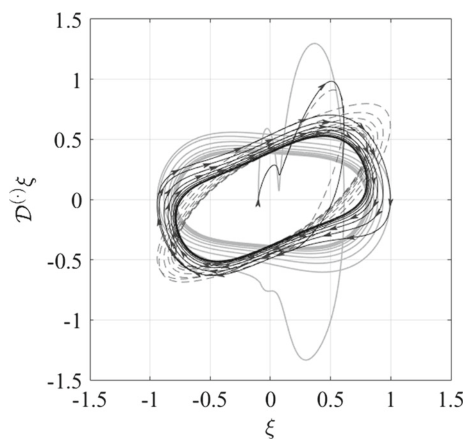

Fig. 5 The same as in Fig. 4, except with $c = 1.89$ for $\tau \in [0, 100]$, and with *arrows* plotted at intervals of $\Delta\tau = 1$ for $\tau \in [0, 50]$

order 1 and order 1/2 phase diagrams. At lower values of c, the VO phase diagram resembles more closely the 1/2 order phase diagram. This is because at lower values of the frictional coefficient, the cart tends to spend more time near the center of the track and the distribution of q is quadratic about the origin in favor of the 1/2 order derivative.

5.3 Stability characteristics of the solution surface

A more complete picture of the system response to the VO frictional effects can be realized by plotting the

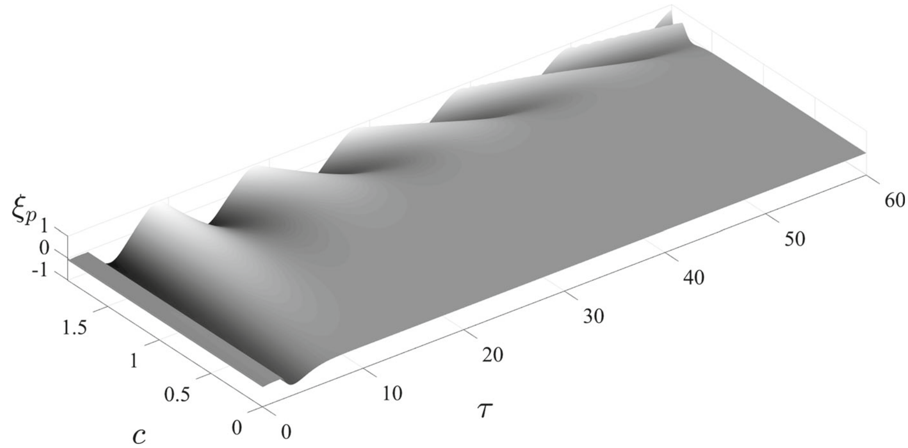

Fig. 6 Cart error dynamics, ξ_p, over the investigated frictional interval, $c \in [0, 1.89]$. Note that the finite horizon is mostly unaffected by increasing values of c, while the infinite horizon exhibits oscillatory behavior for higher frictional values, with increasing amplitude corresponding to increasing c

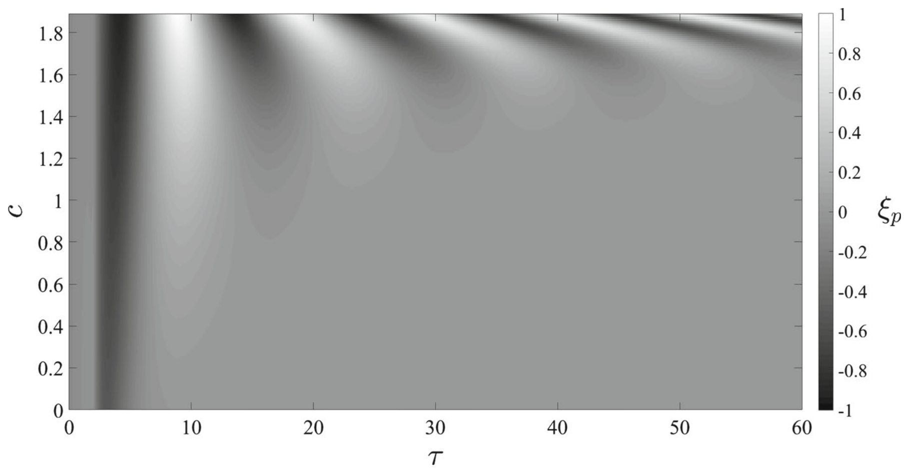

Fig. 7 Cart error dynamics, ξ_p, over the investigated frictional interval, $c \in [0, 1.89]$. The oscillatory behavior of the system for increasing values of c demonstrates a combined continuous phase shift and increase in frequency. The boundary between the region of persistent oscillation and the region of stability exhibits an asymptotic character for $\tau \geq T$

solution error surface, $\xi_p = f(\tau, c)$, over the investigated frictional interval (Fig. 6). The figure makes it clear that increasing the value of c on the given interval has negligible effect on the characteristic system behavior during the finite horizon (even in the presence of an initial error), but a continuous destabilizing effect on the system in the infinite horizon.

The surface mapping of the cart position error dynamics given in Fig. 7 reveals the combination of continuous phase shift and continuous increase in frequency of the oscillations for increasing values of the frictional coefficient (e.g., at $c \approx 1.7$ the system completes 4 periods by $\tau = 60$, whereas at $c = 1.89$ the system completes 5 periods in the same time). This results in the apparent bending of the wavelike structures about the upper τ axis defined by $c = 1.89$. This bending is a result of the dynamic interdependence of the cart position, variable derivative order, and control system response. Another feature of note is the asymptotic character of the boundary between the stable solution region and the region of persisting oscillatory behavior. This suggests a critical value of the frictional coefficient which divides the two regions after the transient swing-up effects have vanished, but before the longtime decay of the oscillations.

6 Stability analysis

The results given in Sect. 5.3 suggest that the controlled system demonstrates persisting oscillatory behavior above some critical value of the frictional coefficient, $c > c_c$. That is, there exists some c_c toward which a margin—between small-amplitude, quickly decaying oscillations and large-amplitude, slowly decaying oscillations—tends. Our goal in the present section is to formulate and solve an eigenvalue expression for the controlled system in order to verify this result. Specifically, we seek an expression of the form

$$\mathcal{F}(s; c) = 0, \tag{25}$$

where $s \in \mathbb{C}$ denotes an eigenvalue of the system. If we let s_c correspond to the most unstable mode, then [20]: if $Re(s_c) < 0$, the system is said to be asymptotically stable; if $Re(s_c) > 0$, the system is said to be unstable; and if $Re(s_c) \equiv 0$, the system is said to be neutrally stable. We employ a linear stability analysis typical of, e.g., fluid mechanical systems and delineated in standard hydrodynamic stability texts such as [20]. We take our analysis on the infinite horizon and define—in the language of hydrodynamic stability—our 'basic' solution, denoted here $\bar{\boldsymbol{\xi}}$, to be the nominal trajectory (which in the infinite horizon is the origin of the state-space). The basic trajectory is generated by the basic control (i.e., the nominal control), denoted here $\bar{u} = 0$.

6.1 Developing the eigenvalue relation, $\mathcal{F}(s; c) = 0$

We define the perturbed state

$$\begin{aligned} \boldsymbol{\xi} &\triangleq \bar{\boldsymbol{\xi}} + \boldsymbol{\xi}', \\ &= \boldsymbol{\xi}', \\ &= \left(\xi' \;\; \theta' \;\; \frac{d\xi'}{d\tau} \;\; \frac{d\theta'}{d\tau}\right)^{\top}, \end{aligned} \tag{26}$$

and the perturbed control

$$\begin{aligned} u &\triangleq \bar{u} + u', \\ &= u', \end{aligned} \tag{27}$$

where the primed quantities are taken to be much less than unity. Substituting the perturbed quantities into Eq. (11), subtracting the nominal solution, and noting that nonlinear primed terms are negligible compared to the other terms (e.g., $\theta'\xi' \approx 0$), we arrive at the perturbation equations

$$\begin{aligned} &\frac{d^2\xi'}{d\tau^2} + \mathcal{T}\frac{d^2\theta'}{v^2} = u' - c\mathcal{D}^{1/2}\xi', \\ &\mathcal{T}\frac{d^2\xi'}{d\tau^2} + \mathcal{I}\frac{d^2\theta'}{d\tau^2} = \gamma\theta'. \end{aligned} \tag{28}$$

That the VODO reduces to a constant half-order operator when linearized about the nominal trajectory will become important in a later analysis of the simulation results. The perturbation control signal is a feedback on the state perturbation, with the optimal feedback gain matrix being $K = (k_\xi \;\; k_\theta \;\; k_{\mathcal{D}^1\xi} \;\; k_{\mathcal{D}^1\theta})$, so that

$$\begin{aligned} u' &= K\boldsymbol{\xi}', \\ &= k_\xi\xi' + k_\theta\theta' + k_{\mathcal{D}^1\xi}\frac{d\xi'}{d\tau} + k_{\mathcal{D}^1\theta}\frac{d\theta'}{d\tau}. \end{aligned} \tag{29}$$

Proceeding with a normal mode analysis, we define our normal modes to be

$$\begin{aligned} \xi' &\triangleq \hat{\xi}e^{s\tau}, \\ \theta' &\triangleq \hat{\theta}e^{s\tau}, \end{aligned} \tag{30}$$

where $\hat{\xi}$ and $\hat{\theta}$ are functions of the ξ-coordinate alone. Then,

$$\begin{aligned} \mathcal{D}^{1/2}\xi' &= \mathcal{D}^{1/2}\hat{\xi}e^{s\tau}, \\ &= [e^{s\tau}\sqrt{s}Erf(\sqrt{s\tau})]\hat{\xi}, \end{aligned} \tag{31}$$

where $Erf(\cdot)$ denotes the error function, and where we have chosen the Caputo definition for evaluation of the semiderivative. The Caputo definition results in an expression that is valid for $\tau = 0$, whereas other, less restrictive operators (e.g., Riemann-Liouville and Grünwald-Letnikov) result in an expression with singular behavior near $\tau = 0$. For large τ—that is, in the infinite horizon—Eq. (31) becomes

$$\lim_{\tau\to\infty}\mathcal{D}^{1/2}\xi' = s^{1/2}\xi'. \tag{32}$$

Substituting Eqs. (29), (30), and (32) into Eq. (28) and dividing out exponential terms, we have

$$\begin{aligned} &s^2\hat{\xi} + \mathcal{T}s^2\hat{\theta} = k_\xi\hat{\xi} + k_\theta\hat{\theta} \\ &\quad + k_{\mathcal{D}^1\xi}s\hat{\xi} + k_{\mathcal{D}^1\theta}s\hat{\theta} - cs^{1/2}\hat{\xi}, \\ &\mathcal{T}s^2\hat{\xi} + \mathcal{I}s^2\hat{\theta} = \gamma\hat{\theta}. \end{aligned} \tag{33}$$

Solving the bottom equation for $\hat{\theta}$, substituting into the top equation, and then dividing through by $\hat{\xi}$ yield the desired eigenvalue relation, $\mathcal{F}(s; c) = 0$, given by the expression

$$\begin{aligned} &(\mathcal{I} - \mathcal{T}^2)s^4 + (\mathcal{T}k_{\mathcal{D}^1\theta} - \mathcal{I}k_{\mathcal{D}^1\xi})s^3 + (\mathcal{I}c)s^{5/2} \\ &\quad + (\mathcal{T}k_\theta - \mathcal{I}k_\xi - \gamma)s^2 + (\gamma k_{\mathcal{D}^1\theta})s \\ &\quad - (\gamma c)s^{1/2} + \gamma k_\xi = 0, \end{aligned} \tag{34}$$

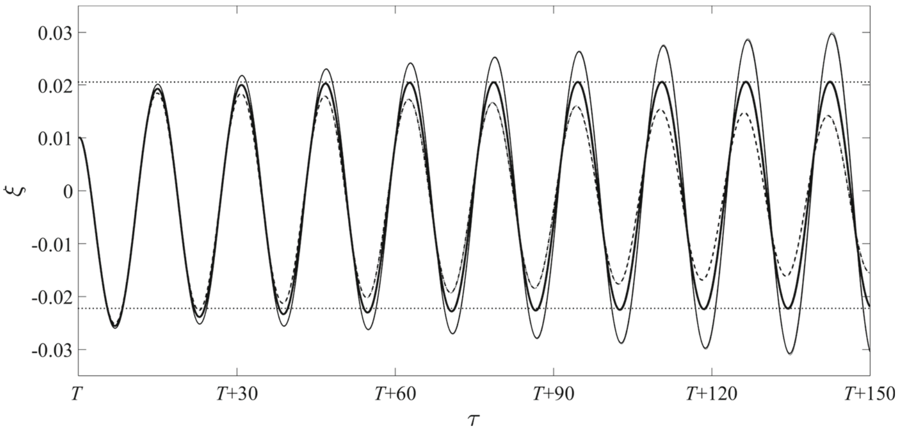

Fig. 8 Simulations run on the infinite horizon starting from rest and with a perturbation on the cart position of $\xi' = 0.01$. *Black lines* correspond to VO simulations and gray lines correspond to FO simulations. In each case, the values $c \in \{1.7199, 1.7299, 1.7399\}$ yield, respectively, the decaying stable oscillation (*dashed lines*), the persistent neutrally stable oscillation (*thick solid lines*), and the growing unstable oscillation (*thin solid lines*). The stable and unstable modes were generated by varying the frictional coefficient, $\Delta c = \pm 0.01$, about the critical value. The VO and FO systems produce essentially identical trajectories, so that the FO system is mostly concealed in the plot. The *dotted horizontal lines* indicate the persistent oscillation amplitude after the transient response has vanished. Note that the limit cycle is not symmetric about the origin, tending away from the initial perturbation until a steady state is reached

where all parameters other than s and c are known. The physical parameters $\mathcal{T}$, $\mathcal{I}$, and γ are known from the outset, whereas the parameters k_ξ, k_θ, $k_{\mathcal{D}^1\xi}$, and $k_{\mathcal{D}^1\theta}$ are resolved (by solving the algebraic Riccati equation) for all $\tau \in [T, \infty)$ once the control tuning parameters have been set. Thus, once one has decided upon a tuning configuration, the above relation can be immediately solved (as will be presently demonstrated) to determine the frictional threshold beyond which the system becomes unstable.

6.2 Theoretical value of the critical frictional coefficient

For the present system, $\mathcal{T} \approx -0.007143$, $\mathcal{I} \approx 0.001429$, $\gamma \approx 0.08460$, $k_\xi \approx 1.0000$, $k_\theta \approx -29.5967$, $k_{\mathcal{D}^1\xi} \approx 1.9995$, and $k_{\mathcal{D}^1\theta} \approx -3.9182$. Upon substitution of these values into Eq. (34) and application of the appropriate root-finding algorithm, one obtains

$$c_c \approx 1.7299, \tag{35}$$

corresponding to $Re(s_c) \approx 0$ for the least stable eigenvalue, s_c.

6.3 Experimental value of the critical frictional coefficient

The eigenvalue relation has been obtained in the infinite horizon and implicitly assumes a state of dynamic equilibrium at the outset of the stabilization period (and for all times previous). This is because the eigenvalue relation does not consider a history input from the finite horizon (swing-up) portion of the problem. Accordingly, we verify the critical value, c_c, with simulations starting at $\tau = T$ from a state of dynamic equilibrium for all $\tau < T$. We apply to the cart's position a perturbation from the nominal trajectory (at the origin of the state-space) of $\xi' = 0.01$. Figure 8 gives the results of simulations run for $c \in \{1.7199, 1.7299, 1.7399\}$. These values were chosen to illustrate concisely the results of a more exhaustive iterative search performed by the authors, leading to the determination of the critical value $c_c = 1.7299$ and confirming the theoretical result. We recall that the derivation of the eigenvalue relation reduces the operator of VO to an operator of constant-order 1/2. For this reason, it is necessary to include in the figure coinciding simulations conducted where the operator of VO q has been replaced with an operator of constant-order 1/2 (physically, this last

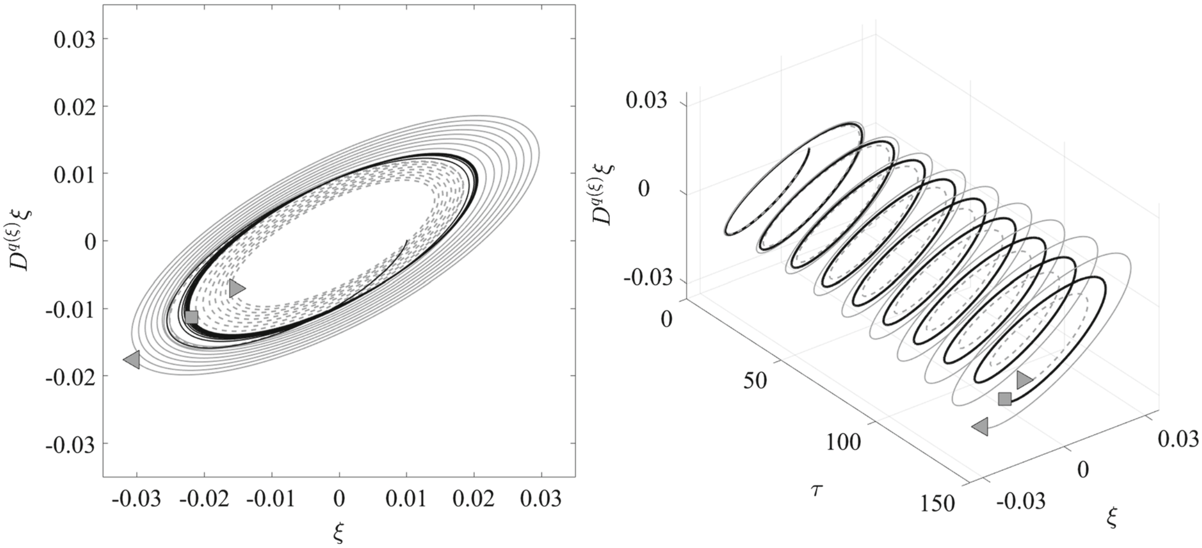

Fig. 9 Two-dimensional (*left*) and three-dimensional (*right*) depictions of the variable phase space of the VO system for the stable (*dashed gray*), neutrally stable (*solid black*), and unstable (*solid gray*) modes corresponding to Fig. 8. The initial states of each coincide; the endpoints indicated in each plot correspond. The trajectory approached by the neutrally stable mode is a true limit cycle

corresponds to a track coated entirely in a viscoelastic film). This is because both of the aforementioned are memory operators, so that deviations from the nominal state are expected to produce a significant aggregate deviation between the two if the displacement is 'large enough'. Since we have used the constant-order semi-derivative to derive the eigenvalue relation, the relation's validity should be dependent on how closely the VO and FO systems behave. For the perturbation noted previously, the behavior of the VO and FO simulations is essentially identical. This is as should be expected, since for both systems these simulations bear out (to four decimal places) the critical value obtained from Eq. (34).

Figure 9 gives the variable phase space for the VO system under the perturbation $\xi' = 0.01$. The limit cycle produced by the critical value $c_c = 1.7299$ clearly defines the boundary between the phase spaces of the stable and unstable modes.

We now conduct the same simulations, except with the starting perturbation $\xi' = 0.1$—an order of magnitude larger than the previous. As expected, with a larger perturbation the VO and FO systems no longer produce identical trajectories (Fig. 10). The result is that the VO system has the modified critical frictional value $c_c = 1.7448$, while the FO system retains its critical value of $c_c = 1.7299$. The error in the estimate of c_c for the VO system using Eq. (34) is less than one percent. Regardless, it is clear that the VO system tends to be stable for higher frictional coefficient values than given by the derived eigenvalue relation under large perturbations (recalling that the relation assumes 'small' perturbations). This is to say that for the actual (VO) system presented here, the critical frictional value is dependent on the perturbation present at the outset of the stabilization period. Finally, we note that the phase shift present in the FO system is constant over time for differing values of c, whereas this is not the case for the VO system since the frequency of the oscillation of the VO system changes for differing values of the frictional coefficient. This is most readily apparent in Fig. 10 by comparing the left-hand (or right-hand) trajectory intersections of the various modes for a given oscillation crest. The perturbation value for these points of intersection does not change over time for the FO system, but does change for the VO system.

6.4 Predictive validity of the eigenvalue relation

We now pose the question of whether the critical frictional value determined using Eq. (34) has utility in providing stability estimates over the entire time horizon (i.e., over the entire swing-up and stabilization

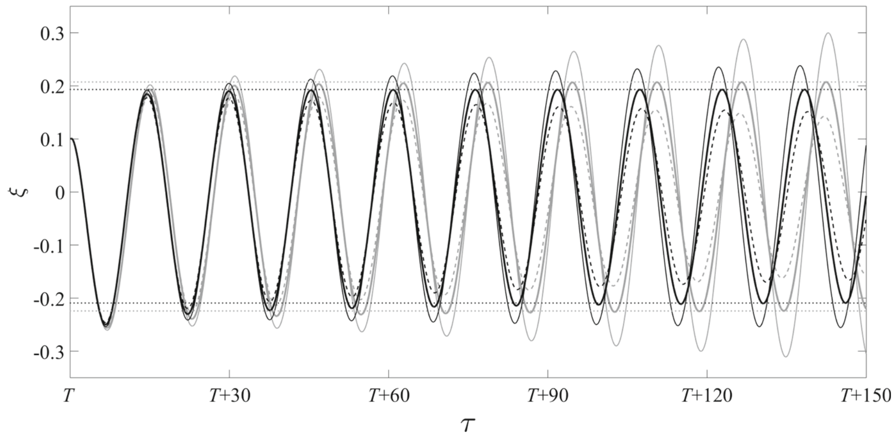

Fig. 10 Simulations run on the infinite horizon starting from rest and with a perturbation on the cart position of $\xi' = 0.1$. Plot indicators are as in Fig. 8, where now $c \in \{1.7348, 1.7448, 1.7548\}$ for the VO system (*black*) and $c \in \{1.7199, 1.7299, 1.7399\}$ for the FO system (*gray*), and where the values of the frictional coefficient are given in the order: stable, marginal, unstable. The stable FO steady-state amplitude (*dotted gray*) encloses the stable VO steady-state amplitude (*dotted black*), indicating that the VO system is less sensitive to increases in c for a given perturbation. This is also apparent when comparing the growth rate (i.e., envelope) of the unstable FO mode (*thin solid gray*) to that of the unstable VO mode (*thin solid black*). Finally note that there is a continuous change in frequency for differing c values of the VO system, whereas the phase shift between c values of the FO system is constant

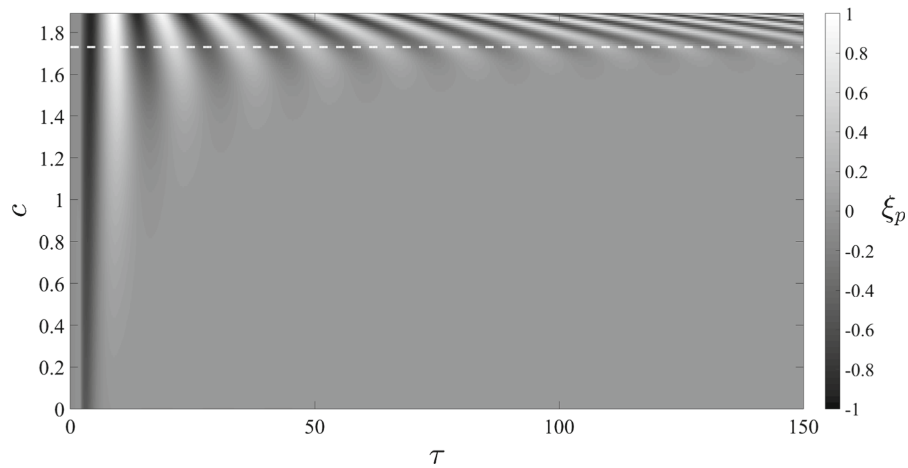

Fig. 11 Cart position over time for $c \in [0, 1.89]$. The dashed line indicates the critical frictional value, $c_c = 1.7299$, obtained from the previously derived eigenvalue relation

process). Figure 11 shows the cart position over time for the entire investigated interval of c. The dashed line representing the critical value, $c_c = 1.7299$, clearly defines a boundary (over 'reasonable' time periods) above which larger oscillations emerge and persist, and below which smaller amplitude oscillations emerge and quickly dissipate. We recall that no true limit cycle emerges, and that—for very large times—all oscillations on the investigated frictional interval will decay to zero. This is a result of the VO dynamics, the history input from the swing-up phase imparted to the stabilization phase, and the significant perturbation received by the stabilizing controller as the initial state of the infinite horizon (recalling that larger perturbations tend to increase the critical value of the frictional coefficient).

7 Conclusions

Over the last three decades, research has revealed the presence of FO behavior in the dynamics of many common physical systems. Recent work in control theory has extended traditional methods for the control of systems described by integer-order differential equations into the domain of those described by constant FO differential equations, often resorting to control methods which themselves are of FO. This work builds upon previous contributions by further extending traditional control methods to systems described by differential equations containing a differential operator of VO. The model equations are developed within the framework of a well-known problem involving the control of nonlinear dynamics with the inclusion of VO damping behavior. The problem is defined over a time-varying finite horizon and a time-invariant infinite horizon.

Using nondimensionalized state-space equations over the time-varying portion of the problem, a model-predictive method is presented for the development of a nominal control solution generating a desirable nominal state trajectory. A complimentary method is presented for development of the time-varying corrective control of deviations from the nominal trajectory. The method is extended to the time-invariant portion of the problem.

An example system is defined, and simulations are conducted using unity weighting for the control system tuning in order to provide a basis of comparison for increasing importance of the VO damping term. Using the proposed methods, stable control solutions are generated for a range of damping term coefficient values. It is shown that increasing importance of the VO damping has a continuous destabilizing effect on the system in the infinite horizon. Further, the dynamic interdependence of the state trajectory, variable derivative order, and feedback response is shown to alter the fundamental oscillatory dynamics of the controlled system.

A method is given for the derivation of a FO eigenvalue relation defining the dependence of the system stability in the infinite horizon on the VO damping coefficient. The relation is used to determine the critical value of the damping coefficient for the example system. Using simulations in the infinite horizon, the critical damping value is confirmed for perturbations from the nominal solution of order much less than unity. It is shown that for larger perturbations from the nominal solution, the critical damping value of the controlled variable order system is dependent on the initial perturbation—a feature distinguishing the VO dynamics from those of constant (fractional or integer) order. The critical value of the damping coefficient obtained from the infinite-horizon eigenvalue relation is compared to simulations run for the entire temporal horizon. It is empirically demonstrated that the analytically obtained critical damping value defines a boundary between solutions that rapidly stabilize to the state-space origin and those which persistently oscillate for longtimes.

References

1. Anastasio, T.J.: The fractional-order dynamics of brainstem vestibulo-oculomotor neurons. Biol. Cybern. **72**(1), 69–79 (1994)
2. Atkinson, K.E.: The numerical solution of Fredholm integral equations of the second kind. SIAM J. Numer. Anal. **4**(3), 337–348 (1967)
3. Bagley, R.L., Calico, R.A.: Fractional order state equations for the control of viscoelastically damped structures. J. Guid. Control Dyn. **14**(2), 304–311 (1991)
4. Balachandran, K., Park, J.Y., Anandhi, E.R.: Local controllability of quasilinear integrodifferential evolution systems in Banach spaces. J. Math. Anal. Appl. **258**(1), 309–319 (2001)
5. Bewley, T.R.: Numerical Renaissance: Simulation, Optimization, and Control. Renaissance Press, San Diego (2014)
6. Boubaker, O.: The inverted pendulum: a fundamental benchmark in control theory and robotics. In: Proceedings of the International Conference on Education and e-Learning Innovations, pp. 1–6 (2012)
7. Bugeja, M.: Non-linear swing-up and stabilizing control of an inverted pendulum system. In: Proceedings of the IEEE Region 8 EUROCON 2003. Computer as a Tool., vol. 2, pp. 437–441 (2003)
8. Calvet, J.P., Arkun, Y.: Stabilization of feedback linearized nonlinear processes under bounded perturbations. In: Proceedings of the American Control Conference (1989)
9. Calvet, J.P., Arkun, Y.: Design of P and PI stabilizing controllers for quasi-linear systems. Comput. Chem. Eng. **14**(4–5), 415–426 (1990)
10. Campbell, S.A., Crawford, S., Morris, K.: Friction and the inverted pendulum stabilization problem. J. Dyn. Sys. Meas. Control **130**(5), 054502-1–054502-7 (2008)
11. Caputo, M.: Linear models of dissipation whose Q is almost frequency independent-II. Geophys. J. R. Astron. Soc. **13**(5), 529–539 (1967)
12. Caputo, M., Mainardi, F.: A new dissipation model based on memory mechanism. Pure Appl. Geophys. **91**(1), 134–147 (1971)
13. Charef, A., Sun, H.H., Tsao, Y.Y., Onaral, B.: Fractal systems as represented by singularity function. IEEE Trans. Autom. Control **37**(9), 1465–1470 (1992)
14. Chen, Y., Liu, L., Li, X., Sun, Y.: Numerical solution for the variable order time fractional diffusion equation with bernstein polynomials. CMES-Comput. Model. Eng. **97**(1), 81–100 (2014)
15. Coimbra, C.F.M.: Mechanics with variable-order differential operators. Ann. Phys. **12**(11–12), 692–703 (2003)
16. Coimbra, C.F.M., L'Espérance, D., Lambert, R.A., Trolinger, J.D., Rangel, R.H.: An experimental study on

stationary history effects in high-frequency Stokes flows. J. Fluid Mech. **504**, 353–363 (2004)
17. Diaz, G., Coimbra, C.F.M.: Nonlinear dynamics and control of a variable order oscillator with application to the van der Pol equation. Nonlinear Dyn. **56**(1–2), 145–157 (2009)
18. Diaz, G., Coimbra, C.F.M.: Dynamics and control of nonlinear variable order oscillators. In: Evans, T. (ed.) Nonlinear Dynamics, Chapter 6, pp. 129–144. InTech, Rijeka (2010)
19. Drazin, P.G.: Nonlinear Systems, 2nd edn. Cambridge University Press, Cambridge (1992)
20. Drazin, P.G., Reid, W.H.: Hydrodynamic Stability, 2nd edn. Cambridge University Press, Cambridge (2004)
21. Durand, S., Guerrero-Castellanos, J.F., Marchand, N., Guerrero-Sánchez, W.F.: Event-based control of the inverted pendulum: swing up and stabilization. J. Control Eng. Appl. Inform. **15**(3), 96–104 (2013)
22. Hartley, T.T., Lorenzo, C.F.: Dynamics and control of initialized fractional-order systems. Nonlinear Dyn. **29**(1), 201–233 (2002)
23. Hwang, C., Leu, J.F., Tsay, S.Y.: A note on time-domain simulation of feedback fractional-order systems. IEEE Trans. Autom. Control **47**(4), 625–631 (2002)
24. Ingman, D., Suzdalnitsky, J., Zeifman, M.: Constitutive dynamic-order model for nonlinear contact phenomena. J. Appl. Mech. **67**(2), 383–390 (1999)
25. Khalil, H.K.: Nonlinear Systems, 3rd edn. Prentice Hall, Upper Saddle River (2002)
26. L'Espérance, D., Coimbra, C.F.M., Trolinger, J.D., Rangel, R.H.: Experimental verification of fractional history effects on the viscous dynamics of small spherical particles. Exp. Fluids **38**(1), 112–116 (2005)
27. Li, Y., Chen, Y.: Fractional order linear quadratic regulator. In: Proceedings of the IEEE/ASME International Conference on Mechatronic and Embedded Systems and Applications, pp. 363–368 (2008)
28. Lorenzo, C.F., Hartley, T.T.: Initialization in fractional order systems. In: Proceedings of the European Control Conference, pp. 1471–1476 (2001)
29. Lorenzo, C.F., Hartley, T.T.: Variable order and distributed order fractional operators. Nonlinear Dyn. **29**(1), 57–98 (2002)
30. Mainardi, F.: Fractional Calculus and Waves in Linear Viscoelasticity: An Introduction to Mathematical Models. Imperial College Press, London (2010)
31. Miller, K.S., Ross, B.: An Introduction to the Fractional Calculus and Fractional Differential Equations. Wiley, New York (1993)
32. Monje, C.A., Chen, Y., Vinagre, B.M., Xue, D., Feliu, V.: Fractional-Order Systems and Controls. Advances in Industrial Control. Springer, London (2010)
33. Oldham, K.B., Spanier, J.: The replacement of Fick's laws by a formulation involving semidifferentiation. J. Electroanal. Chem. Interfacial Electrochem. **26**(2—-3), 331–341 (1970)
34. Oldham, K.B., Spanier, J.: The Fractional Calculus. Academic Press, San Diego (1974)
35. Podlubny, I.: Fractional Differential Equations. Academic Press, San Diego (1999)
36. Podlubny, I.: Fractional-order systems and $PI^{\lambda}D^{\mu}$-controllers. IEEE Trans. Autom. Control **44**(1), 208–214 (1999)
37. Ramirez, L.E.S., Coimbra, C.F.M.: On the selection and meaning of variable order operators for dynamic modeling. Int. J. Differ. Equ. **2010**, Article ID 846107 (2010)
38. Ross, B.: The development of fractional calculus 1695–1900. Hist. Math. **4**(1), 75–89 (1977)
39. Ross, B., Samko, S.G.: Fractional integration operator of variable order in the Hölder spaces $H^{\lambda(x)}$. Int. J. Math. Math. Sci. **18**(4), 777–788 (1995)
40. Samko, S.G., Ross, B.: Integration and differentiation to a variable fractional order. Integral Transforms Spec. Funct. **1**(4), 277–300 (1993)
41. Shen, S., Liu, F., Chen, J., Turner, I., Anh, V.: Numerical techniques for the variable order time fractional diffusion equation. Appl. Math. Comput. **218**(22), 10861–10870 (2012)
42. Soon, C.M., Coimbra, C.F.M., Kobayashi, M.H.: The variable viscoelasticity oscillator. Ann. Phys. **14**(6), 378–389 (2005)
43. Sun, Z., Tsao, T.C.: Control of linear systems with nonlinear disturbance dynamics. In: Proceedings of the American Control Conference, vol. 4, pp. 3049–3054 (2001)
44. Torvik, P.J., Bagley, R.L.: On the appearance of the fractional derivative in the behavior of real materials. J. Appl. Mech. **51**(2), 294–298 (1984)
45. Wang, L., Ma, Y., Yang, Y.: Legendre polynomials method for solving a class of variable order fractional differential equation. CMES-Comput. Model. Eng. **101**(2), 97–111 (2014)
46. Westerlund, S.: Dead matter has memory!. Phys. Scr. **43**(2), 174–179 (1991)
47. Yang, J.H., Shim, S.Y., Seo, J.H., Lee, Y.S.: Swing-up control for an inverted pendulum with restricted cart rail length. Int. J. Control Autom. **7**(4), 674–680 (2009)
48. Zhang, H., Liu, F., Zhuang, P., Turner, I., Anh, V.: Numerical analysis of a new space-time variable fractional order advection-dispersion equation. Appl. Math. Comput. **242**, 541–550 (2014)
49. Zhang, H., Shen, S.: The numerical simulation of space–time variable fractional order diffusion equation. Numer. Math. Theor. Methods Appl. **6**(4), 571–585 (2013)